Evidence in support of a four transmembrane-pore-transmembrane topology model for the *Arabidopsis thaliana* Na^+/K^+ translocating AtHKT1 protein, a member of the superfamily of K^+ transporters

Yasuhiro Kato*, Masao Sakaguchi†, Yasuo Mori‡, Kumiko Saito‡, Tatsunosuke Nakamura§, Evert P. Bakker¶, Yoko Sato*, Shinobu Goshima‖, and Nobuyuki Uozumi*‖**

*Graduate School of Bioagricultural Sciences and ‖Bioscience Center, Nagoya University, Nagoya 464-8601, Japan; †Department of Molecular Biology, Graduate School of Medical Science, Kyushu University, Fukuoka 812-8582, Japan; ‡Department of Information Physiology, National Institute for Physiological Sciences, Okazaki 444-8585, Japan; §Faculty of Pharmaceutical Sciences, Chiba University, Inage-ku, Chiba 263-8522, Japan; and ¶Abteilung Mikrobiologie, Universität Osnabrück, Barbarastrasse 11, D-49076 Osnabrück, Germany

Edited by Lily Y. Jan, University of California, San Francisco, CA, and approved March 16, 2001 (received for review November 22, 2000)

The *Arabidopsis thaliana* AtHKT1 protein, a Na^+/K^+ transporter, is capable of mediating inward Na^+ currents in *Xenopus laevis* oocytes and K^+ uptake in *Escherichia coli*. HKT1 proteins are members of a superfamily of K^+ transporters. These proteins have been proposed to contain eight transmembrane segments and four pore-forming regions arranged in a mode similar to that of a K^+ channel tetramer. However, computer analysis of the AtHKT1 sequence identified eleven potential transmembrane segments. We have investigated the membrane topology of AtHKT1 with three different techniques. First, a gene fusion alkaline phosphatase study in *E. coli* clearly defined the topology of the N-terminal and middle region of AtHKT1, but the model for membrane folding of the C-terminal region had to be refined. Second, with a reticulocyte-lysate supplemented with dog-pancreas microsomes, we demonstrated that *N*-glycosylation occurs at position 429 of AtHKT1. An engineered unglycosylated protein variant, N429Q, mediated Na^+ currents in *X. laevis* oocytes with the same characteristics as the wild-type protein, indicating that *N*-glycosylation is not essential for the functional expression and membrane targeting of AtHKT1. Five potential glycosylation sites were introduced into the N429Q. Their pattern of glycosylation supported the model based on the *E. coli*-alkaline phosphatase data. Third, immunocytochemical experiments with FLAG-tagged AtHKT1 in HEK293 cells revealed that the N and C termini of AtHKT1, and the regions containing residues 135–142 and 377–384, face the cytosol, whereas the region of residues 55–62 is exposed to the outside. Taken together, our results show that AtHKT1 contains eight transmembrane-spanning segments.

HKT1 cDNA from wheat roots has been identified as such by its ability to enable yeast cells with deletions of the K^+-uptake genes *TRK1* and *TRK2* to grow at low K^+ concentrations (1–3). A detailed study of the molecular mechanism of HKT1 revealed that HKT1 mediates Na^+/K^+ cotransport (4, 5). An HKT1 homologous protein isolated from *Arabidopsis thaliana*, AtHKT1, shares 41% of its amino acid sequence with HKT1 and functions as a selective Na^+ transporter in *Xenopus laevis* oocytes and mediates low-affinity K^+ transport in *Escherichia coli* (6). Alignment studies revealed that AtHKT1 and HKT1 belong to a family of K^+ transporter proteins present in eukaryotes and prokaryotes (6–9). Other members of the family are the TRK proteins of fungi (2, 3), KtrB in *Vibrio aliginolyticus* (10), NtpJ in *Enterococcus hirae* (11), TrkH in *E. coli* (12), and the KdpA subunit of the *E. coli* P-type K^+ translocating ATPase Kdp (9, 13). All of these proteins appear to have evolved from a simple, KcsA-like K^+ channel protein of prokaryotes and eukaryotes (7–9, 14, 15). A proposed model predicts that these proteins contain eight transmembrane helices as well as four pore forming regions similar to the pore region of the KcsA protein (7, 8, 16). However, experimental evidence supporting this model has been missing.

Very recently, an alternative topological model has been proposed for HKT1 (17). In the report, the loop in the N-terminal region and the C terminus were determined by epitope tagging in a yeast system. To demonstrate the real topological structure of the plant HKT1 protein, a systematic investigation is now required.

The mechanism of the ion selectivity of HKT1 and AtHKT1 also remains unknown. Despite the high degree of homology between wheat HKT1 and AtHKT1, the wheat HKT1 functions as a Na^+-coupled K^+ transporter, whereas the AtHKT1 functions as a K^+-independent highly selective Na^+ transporter in *X. laevis* oocytes (4–6). Studies exploiting site-directed mutations of HKT1 have identified five residues involved in Na^+ binding or K^+ binding (4, 18, 19). However, their positions with respect to the membrane remains unknown, because pore regions and transmembrane segments of HKT1 have not yet been determined.

The present study addresses the question of the transmembrane topology of AtHKT1 of *A. thaliana.* We used alkaline phosphatase (PhoA) fusion protein expression in *E. coli* (20), glycosylation scanning mutagenesis using an *in vitro* membrane integration system (21), and FLAG-epitope tagging of the two AtHKT1 termini and three of the putative loops. The data obtained promise a better understanding of the structure and function not only of AtHKT1, but also of the other members of the protein family to which AtHKT1 belongs.

Materials and Methods

Expression of AtHKT1-PhoA Fusion Proteins in *E. coli*. Plasmid pPAB404-AtHKT1 (GenBank accession no. AF237672; ref. 6) contains a single *Bam*HI site in front of the *AtHKT1*-start codon. For the construction of *AtHKT1-phoA* gene fusion proteins, 5′-*AtHKT1* portions of various lengths were generated by PCR using a *Bam*HI-site containing oligonucleotide as the sense

This paper was submitted directly (Track II) to the PNAS office.

Abbreviation: PhoA, alkaline phosphatase.

**To whom reprint requests should be addressed. E-mail: uozumi@agr.nagoya-u.ac.jp.

The publication costs of this article were defrayed in part by page charge payment. This article must therefore be hereby marked "*advertisement*" in accordance with 18 U.S.C. §1734 solely to indicate this fact.

primer and distal in-frame primers engineered to contain a *Pst*I site as antisense primers with Takara Ex *Taq* polymerase (Takara, Tokyo). The *Bam*HI- and *Pst*I-digested PCR fragments were cloned into the *Bam*HI and *Pst*I sites of plasmid pPAB404 (13). The PhoA-fusion proteins were expressed in *E. coli* strain UT5600, a commonly used host strain for the measurement of PhoA activity (22, 23). PhoA activity was measured by using the toluidine salt of 5-bromo-4-chloro-3-indolyl-phosphate as substrate (24). *E. coli* membranes were prepared as described (25). AtHKT1-PhoA fusion proteins were detected immunologically by using anti-*E. coli*-PhoA antibody (Rockland, Gilbertsville, PA). The nucleotide sequences of all PCR-generated fragments were verified by DNA sequencing.

***N*-Glycosylation of AtHKT1.** A novel *Nco*I site at the *AtHKT1*-start codon and a novel *Sph*I site behind the stop codon were created by PCR. The *Nco*I- and *Sph*I-digested fragments were then cloned into the *Nco*I and *Sph*I sites of pCITE-2a (Novagen, Madison, WI). The asparagine at position 429 (N429) in AtHKT1 forms a consensus *N*-glycosylation acceptor site. It was replaced by glutamine (Q) by using a two-step PCR procedure (26). To generate novel *N*-glycosylation sites, mutations were introduced into the plasmid encoding the N429Q variant protein. *Aat*II-digested plasmid DNA was used to synthesize cRNA employing the T7 RNA polymerase. *In vitro* translation and translocation by using a rabbit reticulocyte lysate system supplemented with [^{35}S]methionine and dog-pancreas microsomes and the treatment with endoglycosidase H were performed essentially as described (27). Membrane vesicles were recovered by ultracentrifugation (200,000 $\times$ *g*) for 20 min through a cushion containing 0.5 M sucrose, 50 mM Hepes/KOH (pH 7.4) to improve the resolution of SDS/PAGE as well as to remove unintegrated products (21).

Immunodetection of Epitope-Tagged AtHKT1 on HEK293 Cells. To generate a FLAG epitope in the AtHKT1, either the pCI-neo vector (Promega) or the pCMV-Tag4A (Stratagene) was used. *AtHKT1* was subcloned as a *Xho*I/*Ssp*I-digested fragment into the *Xho*I-*Sma*I sites of pCI-neo vector. The DYKDDDDK sequence was substituted for residues 9 and 11, residues 135 and 142, or residues 377 and 384, in the resultant plasmids. To add a FLAG epitope at the C terminus of AtHKT1, the *AtHKT1* fragment encoding 506 residues of the entire AtHKT1 without its termination codon was cloned into the *Bam*HI-*Pst*I sites of pCMV-Tag4A. The *Bam*HI-*Pst*I fragment of *AtHKT1* encoding 506 residues of the entire AtHKT1 with its termination codon was subcloned into the *Bam*HI-*Pst*I sites of pCMV-Tag4A. The DYKDDDDK sequence was substituted for residues 55 and 62 in the resultant plasmid. HEK293 cells (American Type Culture Collection, Manassas, VA) were transfected with the FLAG-tagged AtHKT1 constructs. Transfection was carried out by using the SuperFect Transfection Reagent (Qiagen, Chatsworth, CA). Cells were trypsinized, diluted with DMEM containing 10% FBS, 30 units/ml of penicillin, and 30 μg/ml of streptomycin, and plated onto glass coverslips 18 h after transfection. The cells were then fixed with 4% paraformaldehyde/PBS for 20 min. For permeabilization, the cells were incubated in 0.2% Triton X-100/PBS for 15 min at room temperature. After rinsing with PBS, the cells were preincubated for 1 h with 10% normal goat serum (NGS)/PBS, to prevent nonspecific binding of antibodies, and then successively incubated with 1:1,000 diluted anti-FLAG antibody for 1 h and with FITC-labeled anti-mouse goat antiserum (Jackson ImmunoResearch) for 1 h after being washed with 1% NGS/PBS. Immunostained cells were observed through a confocal laser scanning microscope (LSM 510 from Zeiss) equipped with a krypton/argon laser source. A single wavelength of 488 nm was used for excitation, and the emitted fluorescence at 505 nm was collected through an objective lens with 63$\times$ magnification, and an optical section of 1.1 μm was projected on a single plane.

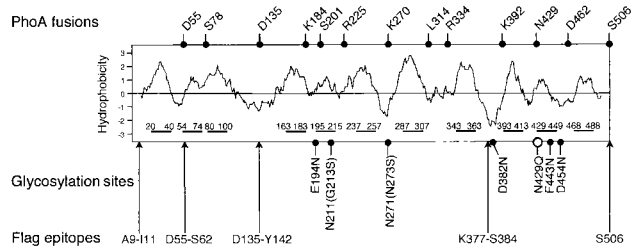

Fig. 1. Schematic representation of the hydrophobic profile of AtHKT1. Hydropathy plot was generated by the method of Kyte and Doolittle (30) with a window of 19 amino acids. Positive values indicate hydrophobic regions. Possible transmembrane segments with 21 amino acids were determined by the TOPPRED II algorithm (31) (lines) and the positions of the ends of the segments are indicated. The positions of the fusion sites selected for PhoA fusions (*Upper*, closed circles), the positions of new glycosylation sites (*Lower*, closed circles), and the positions of Flag epitopes (*Lower*, arrows) are indicated. N429 is a potential endogenous site for *N*-glycosylation (*Lower*, open circle).

Recording of Ion Currents in *X. laevis* Oocytes. The DNA containing the N429Q mutation in AtHKT1 was swapped with the corresponding region in a plasmid for AtHKT1 expression under the control of the T7 promoter (6, 28). Capped complementary RNA encoding wild-type AtHKT1 or N429Q was injected into *Xenopus* oocytes prepared as described (29). The oocytes were kept for 1–2 days at 18°C in a Barth's solution containing 89 mM KCl, 2.4 mM $NaHCO_3$, 0.33 mM $Ca(NO_3)_2$, 0.41 mM $CaCl_2$, 0.82 mM $MgSO_4$, and 10 mM Hepes–NaOH (pH 7.4), before recordings of ionic currents were made by two-electrode voltage clamping. Voltage-pulse protocols, data acquisition, and data analysis were performed by using a voltage clamp amplifier (AxoClamp 2B from Axon Instruments, Foster City, CA). Experiments were performed in a solution containing 6 mM $MgCl_2$, 1.8 mM $CaCl_2$, 100 mM LiCl (or NaCl, KCl, RbCl, CsCl), and 10 mM Mes–1,3-bis[tris(hydroxymethyl)methylamino]propane (BTP) (pH 5.5). The osmolalities (230–250 mosmol/kg) were measured with an osmometer (Advanced Osmometer from Advanced Instruments, Norwood, MA).

Results

Potential Transmembrane Segments in AtHKT1. The deduced amino acid sequence of AtHKT1 was analyzed by using the algorithm of Kyte and Doolittle (30) and the TOPPRED II program developed by von Heijne (ref. 31; Fig. 1). Both programs suggested that AtHKT1 contains eleven potential transmembrane segments, which are distributed at a regular spacing throughout the complete AtHKT1 sequence. One putative endogenous site for *N*-glycosylation (NIT, amino acid residues 429–431) is located at position 429.

AtHKT1-PhoA Fusions. The functional complementation of a K^+ uptake-deficient *E. coli* strain by AtHKT1 suggested that this protein is inserted topologically correctly into the *E. coli* cell membrane (6). Hence, we chose to use fusion constructs with the *E. coli* reporter enzyme PhoA to determine the AtHKT1 topology in the *E. coli* cell membrane (20). PhoA is active only in the periplasm (24). The fusion joints were placed near the C-terminal ends of the predicted exposed loops or in the vicinity of the N-terminal ends of the next presumed transmembrane region (Fig. 1). The PhoA activity data for the various fusion constructs are summarized in Fig. 2. Except for the D462-PhoA protein, all of the AtHKT1 fusions conferring higher PhoA

PHYSIOLOGY

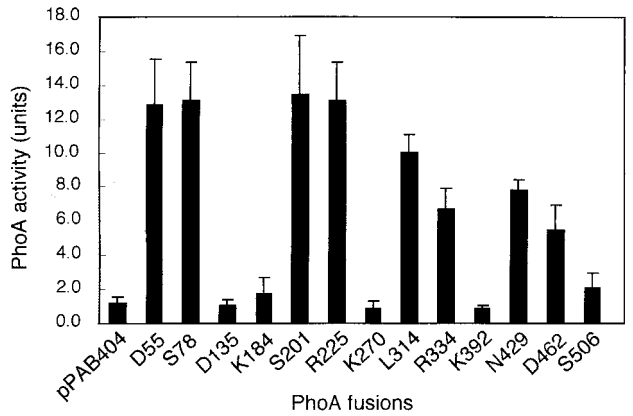

Fig. 2. Enzyme activities of cells containing AtHKT1-PhoA fusions. Data from four to seven transformants of the *E. coli* UT5600 were averaged (±SD) for each AtHKT1 constructs.

activity were present in the membrane fraction as detected by Western blot analysis (Fig. 3). In contrast, the K392-PhoA and S506-PhoA proteins showed little activity (Fig. 2) and were absent from the membrane fraction (Fig. 3). When the PhoA domain of the fusion protein remains in the cytoplasm, it does not form the intrachain disulfide bond essential for activity (24), and it becomes sensitive to proteolytic degradation (24, 32), as has been reported for PhoA-fusion experiments with other ion transporters (13, 25, 33). Some of the degradation may have occurred after the cells were broken for making membranes because all of the intact fusion proteins were detected in samples taken from growing *E. coli* cells (results not shown).

The results in Figs. 2 and 3 are compatible with a model according to which AtHKT1 crosses the membrane eight rather than eleven times (Figs. 1 and 4), because the PhoA fusions at residues D55 and S78, at residues S201 and R225, and at residues N429 and D462 all exhibited high PhoA activity. This suggests that, in contrast to what was expected from the data in Fig. 1, the hydrophobic regions encompassing 54–74, 195–215, and 429–449 shown in Fig. 1 do not constitute transmembrane segments (Fig. 4). On the other hand, there is the observation that the PhoA fusion at residue K184 resulted in low activity (Fig. 2). Position 184 is likely to be located within or near the edge of a transmembrane segment (Fig. 2). The PhoA fusion was constructed to use as a control for the *N*-glycosylation mapping experiment. The details of the location around position 184 will be discussed below.

***N*-Glycosylation at Residue N429.** *N*-glycosylation occurs on the luminal side of the endoplasmic reticulum, which is the extracellular side of the protein when it is disposed to the plasma membrane. To assess whether N429 can be glycosylated, we used

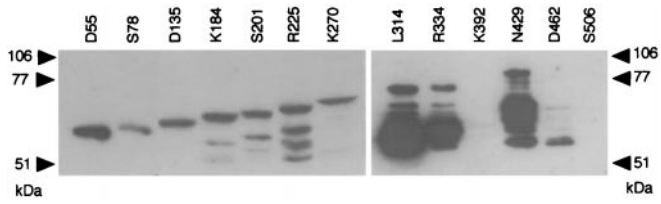

Fig. 3. Immunoblot detection of AtHKT1-PhoA fusion proteins expressed in the *E. coli* UT5600 membrane. Membrane proteins were subjected to SDS/10% PAGE followed by Western blot analysis. D55-PhoA and S78-PhoA, 0.1 μg; K270-PhoA, 5 μg; the remaining PhoA fusions, 1 μg.

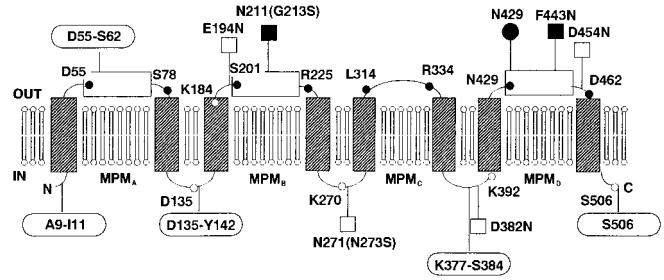

Fig. 4. Topology of the AtHKT1 protein. PhoA-fusion sites, deduced from the results presented in Fig. 2, are shown as closed circles for higher activities and open circles for lower activities. *N*-glycosylated sites or nonglycosylated sites, deduced from the results in Fig. 5, are shown as bars with closed squares or open squares, respectively. The endogenous *N*-glycosylation site at position 429 is indicated by a bar with a closed circle. The positions of the introduction of FLAG epitopes, deduced from the results in Fig. 7 are indicated by bass and ellipse. The hydrophobic regions with the potential to form transmembrane segments (rectangles) are predicted by the TOPPRED II program. The transmembrane segments deduced from the study are indicated as hatched rectangles. The putative positions of MPM$_A$, MPM$_B$, MPM$_C$, and MPM$_D$ were put into the model according to the proposed membrane-pore-membrane (MPM) motif (7).

a cell-free protein synthesis system consisting of a reticulocyte lysate supplemented with dog-pancreas microsomal membranes (21, 27). In the presence of the microsomal membranes, the PAGE profile of AtHKT1 showed an additional band with a higher apparent molecular weight (Fig. 5*A*), which disappeared after treatment with endoglycosidase H (Fig. 5*A*). When the endogenous *N*-glycosylation site was removed by mutating the asparagine at position 429 to a glutamine (N429Q), the upper band did not appear (Fig. 5*A*). These data show that position 429 must be located on the extracellular surface of the cells, which is in agreement with the model based on the results of the PhoA fusions (Fig. 4). The AtHKT1 functionally expressed in *E. coli* must be in an unglycosylated form, but the protein translocated

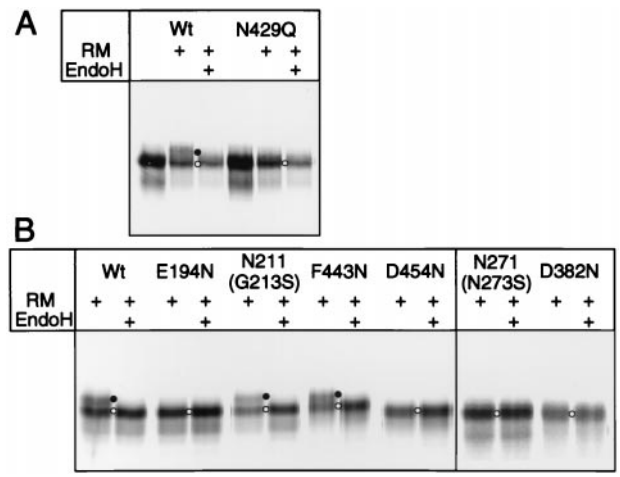

Fig. 5. Detection of *in vitro* translation products for scanning *N*-glycosylation mutagenesis of AtHKT1. (*A*) The proteins wild-type AtHKT1 (Wt) and N429Q were expressed *in vitro* in the absence or presence (+) of rough microsomal membranes from dog pancreas (RM). Aliquots were treated with endoglycosidase H (EndoH). Open and closed circles represent nonglycosylated and glycosylated forms of the protein, respectively. (*B*) The E194N, N211(G213S), N271(N273S), D382N, F443N, and D454N mutants were generated from the N429Q mutant. After the translation reaction in the presence of RM (+), aliquots were treated with endoglycosidase H (EndoH). Symbols are the same as in *A*.

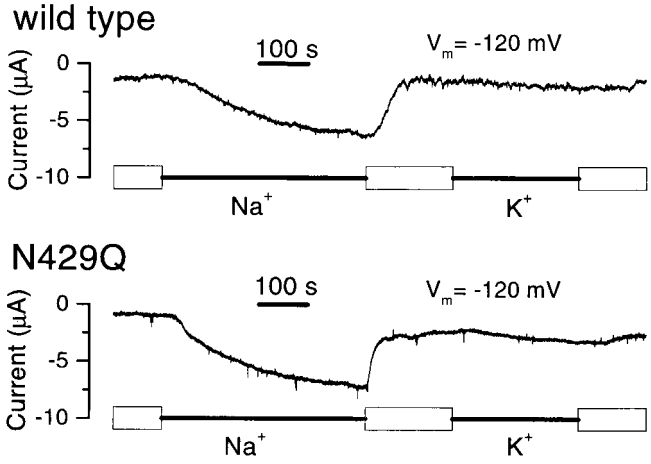

Fig. 6. The N429Q expressed in *Xenopus* oocytes retains selectivity for Na^+. The two electrode voltage clamp experiments were performed with *Xenopus* oocytes expressing wild-type AtHKT1 or N429Q. The membrane potential of the oocytes was held at −120 mV. The bath solution contained 100 mM NaCl or 100 mM KCl.

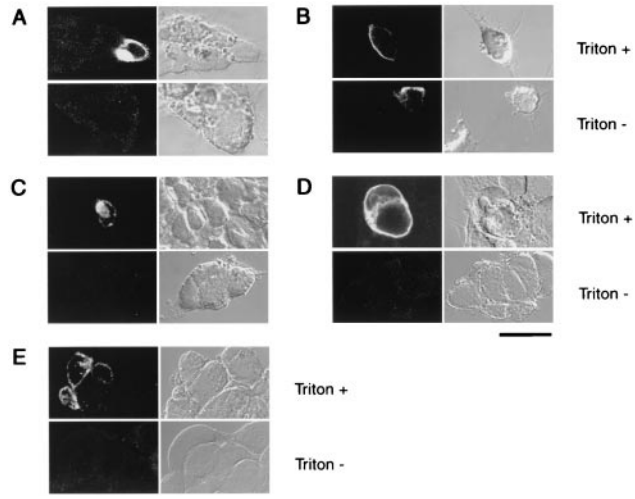

Fig. 7. Immunocytochemical detection of the orientation of the N and C termini and three loops of AtHKT1 recombinantly expressed in HEK293 cells. Cells expressing AtHKT1 constructs tagged with Flag at the N terminus (*A*), the first external loop (D55-S62; *B*), the first internal loop (D135-Y142; *C*), the third internal loop (K377-S384; *D*), and the C terminus (*E*) were tested for accessibility to the Flag epitope of Flag-specific antibody in the presence (Triton +) and absence (Triton −) of Triton X-100. (*Left*) The representative confocal immunoimages; (*Right*) the corresponding differential interference contrast images. (Bar = 20 μm.)

into the dog-pancreas microsomal membranes is the glycosylated form. It has been reported that lack of glycosylation may change membrane topology (34). We tried to determine whether the unglycosylated AtHKT1, N429Q, could be sorted into microsomal membranes in a functional form resembling wild-type AtHKT1. Because it is difficult to measure the ion transport activity of AtHKT1 in dog microsomal membranes, we measured the ion transport capability of the unglycosylated protein (N429Q) in *X. laevis* oocytes by voltage clamp recordings (Fig. 6). The result was similar to that obtained with wild-type AtHKT1 (6) in that both proteins transported Na^+ and did not show detectable K^+ currents (Fig. 6). Moreover, exposure of the oocytes to 100 mM Li^+, Rb^+, or Cs^+ of 100 mM Na^+ or K^+ did not effect the measured current generated by the two proteins (data not shown). These data suggest that the unglycosylated N429Q protein was incorporated into the oocyte plasma membrane without loss of activity, which suggests that the unglycosylated AtHKT1, N429Q, can take up a correct conformation in the dog-pancreas microsomal membranes resembling that of glycosylated AtHKT1. The N429Q was, therefore, used for subsequent experiments.

Mapping the Ends of Transmembrane Segments. The difference in PhoA activity between D462-PhoA and S506-PhoA was relatively small (Fig. 2). In addition, full-length D462-PhoA protein was not detected in the membrane fraction, although the PhoA activity was substantial (Fig. 3). Because of the uncertainty of how to interpret these data, we attempted to clarify the transmembrane topology of the corresponding AtHKT1 region by introducing artificial potential *N*-glycosylation sites (NXS/T) at residues F443, or D454 into the N429Q AtHKT1. Only the F443N-N429Q became *N*-glycosylated (Fig. 5*B*), whereas D454N–N429Q did not show a positive reaction (Fig. 5*B*). An *N*-glycosylation site should be situated at a distance of at least ten residues away from a transmembrane segment for the oligosaccharyl transferase to be able to attach an oligosaccharide to the protein (35, 36). Position 454 is likely to be located too close to a transmembrane segment. To obtain more information on this phenomenon, we investigated different parts of AtHKT1 by generating potential glycosylation sites at position 194 (E194N) or position 211 [N211(G213S)]. E194N-N429Q was not glycosylated (Fig. 5*B*), whereas N211-G213S-N429Q showed a positive reaction (Fig. 5*B*). These data and the PhoA negative activity of K184-PhoA and the positive activity of S201-PhoA (Fig. 2) indicate that the position 194 is located close to a transmembrane segment, and the proposed theory of space requirement for *N*-glycosylation (35, 36) is supported by the results in this study. Thus, we conclude that the positions 454 and 462 are located in the vicinity of the external side of the transmembrane segment encompassing residues 468–488 (Fig. 4).

Another problem on the PhoA results was that the full-length K392-PhoA protein was not detected in the membrane fraction and the amount of K270-PhoA protein was relatively small. To confirm that the corresponding regions face the inside of the membrane, *N*-glycosylation sites were introduced at residue 271 [N271(N273)] or residue 382 (D382) into the N429Q. Neither of the proteins becomes glycosylated (Fig. 5). These results are consistent with the data obtained with K270-PhoA and K392-PhoA.

N Terminus and C Terminus of AtHKT1. Because the short N-terminal and C-terminal tails of AtHKT1 are not suitable for determination of their orientation by the glycosylation scanning method, we expressed AtHKT1 constructs tagged with FLAG epitopes at the N terminus and C terminus in HEK293 cells, testing for accessibility of the epitope to FLAG-specific antibody. When the antibody was applied to the extracellular side of the cells (Fig. 7, Triton −), only signals with intensities equal to those seen without FLAG-specific antibody application were observed (data not shown). In contrast, after the cell membrane was permeabilized by Triton X-100 treatment, confocal images showed intense immunofluorescence at the plasma membrane, which contoured the cells expressing FLAG-tagged ATHKT1 (Fig. 7, Triton +). We verified that expression of AtHKT1 tagged with the Flag epitope at the first external loop (D55-S62) in Figs. 2 and 4 yielded a positive reaction when subjected to staining without the Triton treatment (Fig. 7). These results suggest that the N terminus and C terminus of AtHKT1 face toward the cytosolic space (Fig. 4) and that the region containing D55-S62 faces the outside of the membrane.

Flag Epitope Tagging of the First and Third Internal Loop. Additional constructs with Flag epitope were generated to verify the disposition of the first internal loop (D135-Y142) and of the third internal loop (K377-S384) of AtHKT1 (Fig. 4). In the wheat HKT1, the position corresponding to the first internal loop in AtHKT1 (Fig. 4) was reported to be in the external loop of the membrane (17). Cells expressing Flag-tagged AtHKT1 (D135-Y142) were recognized by the antibody only when they were treated with Triton X-100 (Fig. 7). We conclude that the loop containing D135-Y142 in AtHKT1 faces the intracellular space. The same was observed with cells expressing the Flag tag at the third putative internal loop (K377-S384). Immunofluorescence signals from the permeabilized cells were detected, but no signals were observed with intact, nonpermeabilized cells (Fig. 7). These results with the Flag tags incorporated at different positions in AtHKT1 are in full agreement with those obtained with the PhoA fusion technique (Fig. 2) and with the *N*-glycosylation approach (Fig. 5).

Discussion

Independent experiments using an *E. coli* expression system and PhoA-reporter enzyme fusions (Figs. 2 and 3), glycosylation reactions in a eukaryotic cell-free system (Fig. 5), and HEK293 transfectants and immunofluorescence detection (Fig. 7) provided the data on which we base our topology model of AtHKT1 as shown in Fig. 4. This model is remarkably similar to those proposed for this superfamily of proteins (7–9), in particular with regard to the number of membrane-spanning segments. The data presented here support the notion that the K^+ translocating portion of the K^+ transporter proteins contains only eight and not more transmembrane spanning segments (Fig. 1). According to the proposed membrane-pore-membrane (MPM) motif (7), the MPM_A, MPM_B, MPM_C, and MPM_D were added to the AtHKT1 topology in Fig. 4. The theoretical 4-fold MPM model suggests the existence of an evolutionary link between AtHKT1 as an example of a member of the K^+ transporter family and a two-transmembrane K^+ channel such as KcsA or the inwardly rectifying K^+ channels in animal cells, Kir (14–16). The experimental results of this study, as well as the data presented by Tholema *et al.* (37), strongly support this notion. The latter have shown how important the putative selectivity filter residue Glycine-290 of the third pore region of KtrB from *V. alginolyticus* is. Only the protein variant with alanine at this position was still functional with a 100-fold reduced transport affinity for both K^+ and Na^+.

Five amino acid residues in wheat HKT1 have been identified as being involved in determining Na^+ and K^+ binding affinity (4, 18, 19). According to the topology model of Fig. 4, the residues in AtHKT1 corresponding to these residues 240 and 247, 365, and 464 in the wheat HKT1 are located in the second, third, and fourth external loops in AtHKT1, respectively. The residue corresponding to position 270 in the wheat HKT1 is located in AtHKT1 at the external edge of the fourth transmembrane segment (Fig. 4). Note that according to the model proposed by Durell *et al.* (7) and Tholema *et al.* (37), all of these residues are located inside or close to the putative pore-forming regions.

Several plant membrane proteins, including the *A. thaliana* Shaker-type K^+ channels KAT1 and AKT2 (25, 38), the *A. thaliana* K^+ translocating protein AtKUP1–2 homologs of the *E. coli* K^+ transporter Kup (39), and the *A. thaliana* plastidic ADP/ATP translocator (40) have been found to be functionally expressed in *E. coli* cells. The same appears to be true for AtHKT1 (6). Thus, the results obtained with a combination of different techniques suggest that AtHKT1 folds properly into the *E. coli* cell membrane. We chose the powerful PhoA-fusion approach developed for the determination of the topology of *E. coli* intrinsic membrane proteins (20), which has since been successfully applied to the study of membrane proteins of both animals (41) and plants (25). As the number of transmembrane segments of AtHKT1 were increased in the fusion protein, activity of the putatively outward directed PhoA moiety decreased (Fig. 2). Moreover, some of the longer fusion proteins seemed to be unstable, because we could not find them in the *E. coli* membrane fraction (K392-PhoA, D462-PhoA, and S506-PhoA in Fig. 3). These phenomena have also been observed with other longer PhoA-fusion proteins (13, 33). Nevertheless, the results of the PhoA activity studies of the fusion protein constructs eventually added up and were consistent with the topology model based on the conclusions derived from all of the independent methods used (Fig. 4). Together the results indicate that AtHKT1 can be incorporated into the membranes of animal cells and bacterial cells, and retains the same topology.

It is well known that *N*-glycosylation occurs at the asparagine in a tripeptide (NXS/T) of proteins in plant cells as well as in animal cells, when this sequence is translocated through the endoplasmic reticulum (ER) membrane and accepted by the oligosaccharyl transferase in the ER lumen (42, 43). Space requirements for *N*-glycosylation in extracellular loops have been reported (35, 36). We observed the same requirement in our data of glycosylation at positions 194 and 211 and PhoA fusion at positions 184 and 201 (Figs. 2 and 5). We concluded that positions 429, 443, and 462 are all located on the external side of the membrane as depicted in the model in Fig. 4, and that the transmembrane segment exists around positions 468–488. Note that all positions allocated to the edge of the transmembrane segments in Fig. 1 were predicted based on the assumption of 21 residues composing the transmembrane segments, but they have not yet been determined accurately.

AtHKT1 contains six positively and one negatively charged residues in its hydrophilic N-terminal region between residues 1 and 19. Therefore, it is likely that the first transmembrane segment of AtHKT1 functions as a type II signal-anchor sequence, which mediates the translocation of the N-terminal region, resulting in an N_{cyt}/C_{exo} topology (44–46). This notion is supported by our result showing that the Flag-tagged AtHKT1 N terminus faces the cytoplasm (Fig. 7*A*).

Liu *et al.* (17) propose a ten transmembrane-spanning model for HKT1. They inserted the V5 epitope tagging sequence into loop V129–V187 in HKT1, which corresponds to the first internal loop in AtHKT1 in our study (Fig. 4). They concluded that this loop was located outside of the cell. They also propose that other hydrophobic regions, corresponding to 54–74 and 195–215 on the external side of the membrane in AtHKT1 (Fig. 4), act as transmembrane segments of the wheat HKT1. We think that it is risky to arrive at conclusions about location based on the determination of only one position and by using only one method without determining the locations of neighboring hydrophobic segments. If artifactual or unexpected translocation of the epitope tag occurred accidentally, it would be impossible to notice this. In our study, we found good examples of low activity of PhoA-K184 and nonglycosylation at position 194 (E194N) or position 454 (D454N), which does not fit the final topology of AtHKT1 (Fig. 4) without explanations based on other results. It seems to us that the results from the series of PhoA-fusions and the deductions based on experiments combining different methods paint a more accurate picture. We would, therefore, prefer the topological model as given in Fig. 4. This model will allow further studies to unravel the mechanism of ion transport by members of the K^+ transporter family.

We thank M. Lynn Lamoreux for reading the manuscript. This work was supported by a grants-in-aid for scientific research from the Ministry of Education, Science, Sports and Culture of Japan [122206042, 12019227, and 11660082 (to N.U.) and 11480168 and 10558104 (to M.S.)].

1. Schachtman, D. P. & Schroeder, J. I. (1994) *Nature (London)* **370,** 655–658.
2. Gaber, R. F., Styles, C. A. & Fink, G. R. (1988) *Mol. Cell. Biol.* **8,** 2848–2859.
3. Ko, C. H. & Gaber, R. F. (1991) *Mol. Cell. Biol.* **11,** 4266–4273.
4. Rubio, F., Gassmann, W. & Schroeder, J. I. (1995) *Science* **270,** 1660–1663.
5. Gassmann, W., Rubio, F. & Schroeder, J. I. (1996) *Plant J.* **10,** 869–882.
6. Uozumi, N., Kim, E. J., Rubio, F., Yamaguchi, T., Muto, S., Tsuboi, A., Bakker, E. P., Nakamura, T. & Schroeder, J. I. (2000) *Plant Physiol.* **122,** 1249–1259.
7. Durell, S. R., Hao, Y., Nakamura, T., Bakker, E. P. & Guy, H. R. (1999) *Biophys. J.* **77,** 775–788.
8. Durell, S. R. & Guy, H. R. (1999) *Biophys. J.* **77,** 789–807.
9. Durell, S. R., Bakker, E. P. & Guy, H. R. (2000) *Biophys. J.* **78,** 188–199.
10. Nakamura, T., Yuda, R., Unemoto, T. & Bakker, E. P. (1998) *J. Bacteriol.* **180,** 3491–3494.
11. Takase, K., Kakinuma, S., Yamato, I., Konishi, K., Igarashi, K. & Kakinuma, Y. (1994) *J. Biol. Chem.* **269,** 11037–11044.
12. Schlösser, A., Meldorf, M., Stump, S., Bakker, E. P. & Epstein, W. (1995) *J. Bacteriol.* **177,** 1908–1910.
13. Buurman, E. T., Kim, K.-T. & Epstein, W. (1995) *J. Biol. Chem.* **270,** 6678–6685.
14. Doyle, D. A., Cabral, J. M., Pfuetzner, R. A., Kuo, A., Gulbis, J. M., Cohen, S. L., Chait, B. T. & MacKinnon, R. (1998) *Science* **280,** 69–77.
15. Kubo, Y., Baldwin, T. J., Jan, Y. N. & Jan, L. Y. (1993) *Nature (London)* **362,** 127–133.
16. Jan, L. Y. & Jan, Y. N. (1994) *Nature (London)* **371,** 119–122.
17. Liu, W., Schachtman, D. P. & Zhang, W. (2000) *J. Biol. Chem.* **275,** 27924–27932.
18. Rubio, F., Schwarz, M., Gassmann, W. & Schroeder, J. I. (1999) *J. Biol. Chem.* **274,** 6839–6847.
19. Diatloff, E., Kumar, R. & Schachtman, D. P. (1998) *FEBS Lett.* **432,** 31–36.
20. Manoil, C. & Beckwith, J. (1986) *Science* **233,** 1403–1408.
21. Ota, K., Sakaguchi, M., von Heijne, G., Hamasaki, N. & Mihara, K. (1998) *Mol. Cell* **2,** 495–503.
22. Bibi, E., Gros, P. & Kaback, H. R. (1993) *Proc. Natl. Acad. Sci. USA* **90,** 9209–9213.
23. Enomoto, H., Unemoto, T., Nishibuchi, M., Padan, E. & Nakamura, T. (1998) *Biochim. Biophys. Acta* **1370,** 77–86.
24. Derman, A. I. & Beckwith, J. (1991) *J. Bacteriol.* **173,** 7719–7722.
25. Uozumi, N., Nakamura, T., Schroeder, J. I. & Muto, S. (1998) *Proc. Natl. Acad. Sci. USA* **95,** 9773–9778.
26. Higuchi, R. (1990) in *PCR Protocols*, eds. Innis, M. S., Gelfand, D. H., Sninsky, J. J. & White, T. J. (Academic, Orlando, FL), pp. 177–183.
27. Ota, K., Sakaguchi, M., Hamasaki, N. & Mihara, K. (1998) *J. Biol. Chem.* **273,** 28286–28291.
28. Uozumi, N., Gassmann, W., Cao, Y. & Schroeder, J. I. (1995) *J. Biol. Chem.* **270,** 24276–24281.
29. Schachtman, D. P., Schroeder, J. I., Lucas, W. J., Anderson, J. A. & Gaber, R. F. (1992) *Science* **258,** 1654–1658.
30. Kyte, J. & Doolittle, R. F. (1982) *J. Mol. Biol.* **157,** 105–132.
31. von Heijne, G. (1992) *J. Mol. Biol.* **225,** 487–494.
32. Akiyama, Y. & Ito, K. (1989) *J. Biol. Chem.* **264,** 437–442.
33. Blount, P., Sukharev, S. I., Moe, P. C., Schroeder, M. J., Guy, H. R. & Kung, C. (1996) *EMBO J.* **15,** 4798–4805.
34. Goder, V., Bieri, C. & Spiess, M. (1999) *J. Cell Biol.* **147,** 257–267.
35. Popov, M., Tam, L. Y., Li, J. & Reithmeier, R. A. F. (1997) *J. Biol. Chem.* **272,** 18325–18332.
36. Nilsson, I., Sääf, A., Whitley, P., Gafvelin, G., Waller, C. & von Heijne, G. (1998) *J. Mol. Biol.* **284,** 1165–1175.
37. Tholema, N., Bakker, E. P., Suzuki, A. & Nakamura, T. (1999) *FEBS Lett.* **450,** 217–220.
38. Uozumi, N. (2001) *Am. J. Physiol.*, in press.
39. Kim, E. J., Kwak, J. M., Uozumi, N. & Schroeder, J. I. (1998) *Plant Cell* **10,** 51–62.
40. Tjaden, J., Schwöppe, C., Möhlmann, T., Quick, P. W. & Neuhaus, H. E. (1998) *J. Biol. Chem.* **273,** 9630–9636.
41. Henn, D. K., Baumann, A. & Kaupp, U. B. (1995) *Proc. Natl. Acad. Sci. USA* **92,** 7425–7429.
42. Lerouge, P., Cabanes-Macheteau, M., Rayon, C., Fischette-Lainé, A.-C., Gomord, V. & Faye, L. (1998) *Plant Mol. Biol.* **38,** 31–48.
43. Koizumi, N., Ujino, T., Sano, H. & Chrispeels, M. J. (1999) *Plant Physiol.* **121,** 353–361.
44. von Heijne, G. (1986) *EMBO J.* **5,** 1335–1342.
45. Sato, T., Sakaguchi, M., Mihara, K. & Omura, T. (1990) *EMBO J.* **9,** 2391–2397.
46. Sakaguchi, M., Tomiyoshi, R., Kuroiwa, T., Mihara, K. & Omura, T. (1992) *Proc. Natl. Acad. Sci. USA* **89,** 16–19.